Rapid Musculoskeletal MRI in 2021: Clinical Application of Advanced Accelerated Techniques

Jan Fritz, MD[1], Roman Guggenberger, MD[2], Filippo Del Grande, MD[3]

Musculoskeletal Imaging · Review

Keywords

acceleration, compressed sensing, MRI, simultaneous multislice, synthetic MRI

Submitted: Feb 3, 2020
Revision requested: Feb 14, 2020
Revision received: May 18, 2020
Accepted: May 31, 2020

J. Fritz received institutional research support from Siemens Healthcare USA, DePuy, Zimmer, Microsoft, BTG International, SyntheticMR, and Quality Electrodynamics; served as a scientific advisor to Siemens Healthcare USA, GE Healthcare Technologies, and BTG International; received a speaker's honorarium from Siemens Healthcare USA and GE Healthcare; and has shared patents with Siemens Healthcare and Johns Hopkins University. R. Guggenberger and F. Del Grande received institutional research support from Siemens Healthcare.

OBJECTIVE. The purpose of this article is to provide a practice-focused review of the clinical application of advanced acceleration techniques for rapid musculoskeletal MRI examinations.

CONCLUSION. Parallel imaging, simultaneous multislice acquisition, compressed sensing–based sampling, and synthetic MRI techniques provide unprecedented opportunities for rapid musculoskeletal MRI examinations. For 2D and 3D fast spin-echo and turbo spin-echo pulse sequences, acceleration factors between 3 and 8 can be realized in clinical practice, amounting to a time savings of 66–85% when compared with unaccelerated acquisitions.

Use of a field strength of 3 T, compact echo trains afforded by high-performance gradients, short radiofrequency pulses, high receiver bandwidth, matrix resolution phase undersampling, partial Fourier phase sampling, and matrix interpolation allows acceleration of fast spin-echo (FSE) and turbo spin-echo (TSE) pulse sequences [1]. However, acceleration factors greater than 2 may be difficult to achieve. The additional use of advanced acceleration techniques, such as parallel imaging (PI), simultaneous multislice (SMS) acquisition, compressed sensing (CS)–based sampling, and synthetic MRI techniques, permits musculoskeletal MRI examinations with acceleration factors of 3–8.

The purpose of this article is to provide a practice-focused review of the clinical applications of advanced acceleration techniques for rapid musculoskeletal MRI examinations.

Associations Between Acquisition Time and Acceleration Techniques

PI, SMS acquisition, CS-based sampling, and elliptical scanning are acceleration techniques that shorten acquisition time in a linear fashion. Similar to the use of widely accessible acceleration techniques [1], in practice the use of simplified, proportional relationships can be helpful for estimating the effects of techniques when applied in isolation or in combination, as is shown by the following equation:

$$Acquisition\ time \approx \frac{1}{PI_y \times PI_{SL} \times SMS \times ES \times CS'}$$

where PI_y denotes the PI acceleration factor in the in-plane, phase-encoding direction; PI_{SL} represents the PI acceleration factor in the slice phase-encoding direction (and applies to 3D acquisitions only); *SMS* indicates the SMS acceleration factor (and applies to 2D acquisitions only); *ES* is the undersampling of peripheral phase-encoding information in an elliptical fashion; and *CS* is the CS-based undersampling acceleration factor. The acceleration factors of the advanced acceleration techniques are inversely proportional to the acquisition time, and the combination of techniques results in the multiplication of individual acceleration factors.

Parallel Imaging Acceleration of 2D MRI

How It Works

PI acceleration is one of the most accessible and easy-to-use advanced acceleration techniques for rapid musculoskeletal MRI examinations. PI techniques save acquisition time through sampling only every second phase-encoding step (twofold acceleration) or every third phase-encoding step (threefold acceleration) (Fig. 1) while keeping the FOV,

[1]Department of Radiology, Division of Musculoskeletal Radiology, NYU Grossman School of Medicine, 660 1st Ave, 3rd Fl, Rm 313, New York, NY 10016. Address correspondence to J. Fritz (jan.fritz@nyulangone.org).

[2]Department of Diagnostic and Interventional Radiology, University Hospital Zurich, Zurich, Switzerland.

[3]Department of Radiology, Radiology Clinic, Imaging Institute of Southern Switzerland, Lugano, Ticino, Switzerland.

doi.org/10.2214/AJR.20.22902

AJR 2021; 216:1–16

ISSN-L 0361–803X/21/2163–1

TABLE 1: Effects of Parallel Imaging (PI) Acceleration on Acquisition Time of Sagittal Proton Density–Weighted Turbo Spin-Echo MR Images of the Knee

Parameter	No Acceleration	Twofold Acceleration	Threefold Acceleration
Orientation	Sagittal	Sagittal	Sagittal
Gradient performance	High	High	High
Radiofrequency speed	Fast	Fast	Fast
Minimum TR (ms)	4010	4010	4010
TE (ms)	27	27	27
Echo-train length	12	12	12
Bandwidth (Hz/pixel)	395	395	395
FOV (mm)	150 × 150	150 × 150	150 × 150
Matrix size	386 × 386	386 × 386	386 × 386
Slice thickness (mm)	2.5	2.5	2.5
Voxel size (mm)	0.4 × 0.4 × 2.5	0.4 × 0.4 × 2.5	0.4 × 0.4 × 2.5
No. of slices	30	30	30
No. of concatenations	1	1	1
PI acceleration factor	1	2	3
Phase direction	Head to foot	Head to foot	Head to foot
Phase oversampling (%)	75	75	75
Flip angle (°)	150	150	150
Echo spacing (ms)	8.6	8.6	8.6
Acquisition time	3 min 50 s	2 min 2 s	1 min 26 s

matrix size, and spatial resolution unchanged [2]. The number of omitted phase-encoding steps is directly proportional to the reduced acquisition time (see equation 1). Whereas partial Fourier phase undersampling is methodologically limited to acceleration factors of less than 2, PI can accelerate clinical musculoskeletal MRI examinations by factors of 2 and even 3 (Fig. 2 and Table 1).

Practical Considerations

PI acceleration requires the use of multichannel array coils, which consist of multiple smaller coil elements in specific arrangement patterns [2]. The combination of multiple smaller surface coils and parallel acquisition of MR signals offers several advantages for musculoskeletal MRI (Fig. 3), including a higher overall signal-to-noise ratio (SNR) compared with that observed with the use of single-channel coils and better anatomic coil coverage with smaller air gaps because the smaller coil elements permit building of the coils into anatomic shapes, such as for the foot, hand, and shoulder.

Most PI techniques require either previously obtained or integrated reference scans [2], which deliver information about the origin of the MR signals received in parallel (Fig. 3). Because reference scans require additional acquisition time, the actual PI-accelerated acquisition time is often longer than the original acquisition time divided by the PI acceleration factor (see equation 1). In certain situations, no reference scans are needed.

Many different acronyms exist for PI (Table 2). The differences are usually small. Sensitivity encoding (SENSE, Philips Healthcare or Siemens Healthcare] or mSENSE [Siemens Healthcare])–based techniques [3] may be slightly faster and may yield slightly higher SNRs. GRAPPA–based techniques [4] avoid artifacts with smaller FOVs and exhibit less motion sensitivity when a previous reference scan is used [5].

Although the number of omitted phase-encoding steps reduces the acquisition time, it also results in SNR loss, which is inversely proportional to the square root of the acceleration factor. For example, twofold acceleration results in approximately 30–35% less SNR for musculoskeletal structures. However, many FSE and TSE pulse sequences have an abundance of SNR and afford twofold or even threefold PI acceleration with little perceptible loss of image quality (Fig. 2).

Aside from the SNR threshold of diagnostic image quality, the maximally possible PI acceleration factor also depends on the geometric pattern of the coil elements. The acceleration factor should not exceed the number of coil elements across the phase-encoding direction. If this number is exceeded, degrading aliasing artifacts and noise enhancement may occur. For example, in a 15-channel knee coil that consists of three rings in a head-to-foot direction, PI acceleration with a factor of 4 likely will result in additional aliasing artifacts.

PI and partial Fourier phase acceleration can be combined synergistically. PI acceleration is neutral, whereas partial Fourier phase acceleration can be used to reduce the minimum required TR, which can be especially beneficial for musculoskeletal MRI protocols that consist of T1-weighted pulse sequences (Table 3).

Musculoskeletal Applications

A previous series of studies evaluated the diagnostic performance of PI-accelerated musculoskeletal MRI examinations of

TABLE 2: Vendor-Specific Acceleration Techniques

Acceleration Technique	Canon Medical Systems	GE Healthcare	Hitachi Healthcare	Philips Healthcare	Siemens Healthcare
Parallel imaging					
Image based	Speeder	ASSET	RAPID	SENSE	SENSE and mSENSE
k-Space based	NA	ARC	k-RAPID	kt-SENSE	GRAPPA and CAIPIRINHA
Compressed sensing	Compressed Speeder	HyperSense	NA	Compressed SENSE	Compressed sensing
SMS acceleration	MultiBand Speeder	HyperBand	Dual-Slice	Multiband SENSE	SMS acquisition
3D FSE sequences	mVox	Cube	isoFSE	3D View	SPACE

Note—ASSET = array spatial sensitivity encoding technique, RAPID = rapid acquisition through parallel imaging design, SENSE = sensitivity encoding, mSENSE = modified SENSE, NA = not applicable, ARC = autocalibrating reconstruction for Cartesian imaging, k-RAPID = k-space–based RAPID, k = phase-encode index, t = time, CAIPIRINHA = controlled aliasing in parallel imaging results in higher acceleration, SMS = simultaneous multislice, FSE = fast spin-echo, mVox = multivoxel, isoFSE = isotropic fast-spin echo sequence.

native joints, with surgical inspection used as the reference standard [6–10].

A twofold GRAPPA-accelerated, 8-minute protocol for FSE and TSE MRI of the knee performed at a field strength of 1.5 T showed surgically validated diagnostic accuracies of 87–100% for the detection of internal derangement, which were similar to the diagnostic performances of longer traditional and unaccelerated 2D FSE and TSE MRI protocols [6].

Using an early version of PI, twofold acceleration of fat-suppressed T2-weighted 2D FSE and TSE pulse sequences reduced the duration of knee and shoulder MRI protocols performed at 1.5 T by 50% (to approximately 6–7 minutes) and showed surgically validated diagnostic accuracies similar to that of unaccelerated MRI [7, 8].

A study evaluating twofold PI-accelerated 1.5-T and 3-T protocols for MRI of the knee, each with an acquisition time of 10 minutes, including native proton density (PD)–weighted, T2-weighted,

TABLE 3: Effects of Combined Use of PI Acceleration and Partial Fourier Phase Undersampling on Acquisition Time of Coronal T1-Weighted Turbo Spin-Echo MR Images of the Knee

Parameter	No Acceleration	2.5-Fold Acceleration
Gradient performance	High	High
Radiofrequency speed	Fast	Fast
Minimum TR (ms)	582	461
TE (ms)	8	8
Echo-train length	4	4[a]
Bandwidth (Hz/pixel)	397	397
FOV (mm)	150 × 150	150 × 150
Matrix size	386 × 386	386 × 386
Slice thickness (mm)	3	3
Voxel size (mm)	0.4 × 0.4 × 3.0	0.4 × 0.4 × 3.0
Slices	28	28
Concatenations[b]	2	2
Partial Fourier phase sampling (%)	—	75
PI acceleration factor	—	2
Phase direction	Head to foot	Head to foot
Phase oversampling (%)	75	75
Flip angle (°)	150	150
Echo spacing (ms)	8.6	8.6
Acquisition time	3 min 17 s	1 min 21 s

Note—Dash (—) denotes not applied. PI = parallel imaging.

[a]The new timing afforded by partial Fourier phase sampling would permit an increase in echo-train length from a maximum of 4–5 and an acquisition time of 2 minutes 5 seconds. However, an echo-train length of 5 would result in a small increase in T2 weighting and thus may be avoided to preserve sufficient T1 weighting of the resulting MR images.

[b]Two concatenations indicate that the total number of slices were acquired in two sets.

T1-weighted, and fat-suppressed, PD-weighted TSE pulse sequences found similar diagnostic performances for internal derangement between accelerated and unaccelerated MRI protocols [11, 12].

In combination with reduced TRs and spatial resolution, twofold PI acceleration of 2D FSE and TSE pulse sequences enabled the creation of abbreviated 5-minute protocols for knee and shoulder MRI performed at 1.5 T and 3 T, which were found to be statistically interchangeable with unaccelerated MRI protocols [9, 10].

Threefold PI acceleration has been successfully applied to accelerate advanced metal artifact reduction MRI examinations of the hip [13] and knee [14]. The acceleration reduced the acquisition time of axial, sagittal, and coronal T1-weighted and STIR slice encoding for metal artifact correction (SEMAC) pulse sequences to clinically feasible acquisition times of 5–6 minutes.

Parallel Imaging Acceleration of 3D MRI

How It Works

Similar to 2D MRI, PI reduces the acquisition time of 3D pulse sequences by undersampling phase-encoding information. Because 3D FSE and TSE pulse sequences have two phase-encoding directions (Fig. 4), the baseline acquisition times of 3D pulse sequences are much longer for musculoskeletal MRI applications with high spatial resolution (see equation 1). However, PI acceleration can be performed in both phase-encoding directions (Fig. 4), which leads to multiplication of the acceleration factors. For example, multiplying twofold PI acceleration in the in-plane phase-encoding direction by twofold acceleration in the slice phase-encoding direction produces fourfold acceleration (Fig. 4). Therefore, PI is an an essential acceleration technique for 3D FSE and TSE pulse sequences, PI achieves clinically feasible acquisition times of 5 minutes and less [15] (Table 4 and Fig. 5).

Practical Considerations

Although multiplication of bidirectional acceleration schemes leads to higher accelerations that can drastically reduce the acquisition time of 3D pulse sequences (Fig. 4), associated SNR loss occurs in the same proportion as that observed in 2D MRI. For example, fourfold 3D acceleration results in an SNR loss of approximately 50–60%. However, the volume excitation of 3D pulse sequences yields a much higher baseline SNR than the slice-by-slice excitation of 2D pulse sequences, which compensates for the SNR loss associated with higher acceleration factors. Modern versions of accelerated 3D FSE and TSE pulse sequences can acquire isotropic datasets with spatial resolutions of 0.5–0.6 mm^3 within 5 minutes or less [16–20]. Three-dimensional FSE and TSE pulse sequences are most suitable for peripheral joints because of the availability of transmit-receive coils and less adjacent tissue, both of which avoid phase wrap artifacts in the slice direction.

TABLE 4: PI and Compressed Sensing Acceleration on Acquisition Time Using Sagittal Proton Density–Weighted 3D TSE MR Images of the Knee

Parameter	Fourfold Acceleration of 3D CAIPIRINHA SPACE TSE		Sixfold Acceleration of 3D Compressed Sensing SPACE TSE	
Contrast	PD-Weighted	T2-Weighted with FS	PD-Weighted	T2-Weighted with FS
Orientation	Sagittal	Sagittal	Sagittal	Sagittal
Gradient performance	High	High	High	High
Radiofrequency speed	Fast	Fast	Fast	Fast
TR (ms)	900	1000	1100	900
TE (ms)	28	108	29	92
Echo-train length	60	44	46	36
Bandwidth (Hz/pixel)	422	416	410	410
FOV (mm)	160 × 160	160 × 160	160 × 160	160 × 160
Matrix size	320 × 320	256 × 256	320 × 320	320 × 320
Slice thickness (mm)	0.5	0.6	0.5	0.5
Voxel size (mm)	0.5 × 0.5 × 0.5	0.6 × 0.6 × 0.6	0.5 × 0.5 × 0.5	0.5 × 0.5 × 0.5
No. of slices	240	192	240	240
PI acceleration factor	CAIPIRINHA 2 × 2 shift 1	CAIPIRINHA 2 × 2 shift 1	Sixfold CS	Sixfold CS
Phase direction	Anterior to posterior	Anterior to posterior	Anterior to posterior	Anterior to posterior
Phase oversampling (%)	20	25	12	9
Flip angle (°)	Variable	Variable	Variable	Variable
Echo spacing (ms)	5.6	5.1	5.4	5.3
Acquisition time	4 min 41 s	4 min 45 s	4 min 28 sec	4 min 36 sec

Note—PI = parallel imaging, TSE = turbo spin-echo, CAIPIRINHA = controlled aliasing in parallel imaging results in higher acceleration (Siemens Healthcare), PD = proton density, FS = fat suppression, CS = compressed sensing.

Musculoskeletal Applications

Compared with 2D FSE and TSE pulse sequences, 3D FSE and TSE pulse sequences have undergone a remarkable evolution over time, showing a diagnostic performance similar to that of 2D FSE and TSE pulse sequences in detecting anterior cruciate ligament tears, meniscus tears, and articular cartilage defects [21–23].

In a study investigating 3D MR arthrography of the shoulder, twofold SENSE acceleration of a fat-suppressed, T1-weighted, 3D gradient-echo pulse sequence with isotropic voxel size and an acquisition time of 5 minutes 32 seconds enabled diagnosis of glenoid labral lesions with a surgically confirmed diagnostic performance similar to that of a 2D MR arthrography protocol with an acquisition time of 16 minutes 40 seconds [24].

When compared with a 2D knee MRI protocol with an acquisition time of 12 minutes, a twofold GRAPPA-accelerated, fat-suppressed, PD-weighted 3D SPACE TSE pulse sequence with an acquisition time of 10 minutes showed similar performance in diagnosing internal derangement [25].

Threefold autocalibrating reconstruction for Cartesian imaging (ARC, GE Healthcare)–accelerated, fat-suppressed, PD-weighted 3D variable flip angle (Cube, GE Healthcare) FSE MRI of the knee with an acquisition time of 5 minutes and an isotropic resolution of 0.7 mm showed surgically confirmed diagnostic accuracies of 80–100% for the detection of ligament tears, which were similar to those observed with use of the 2D FSE MRI protocol with a 17-minute acquisition time [26].

To achieve fourfold acceleration of 3D FSE and TSE sequences, PI can be combined with the controlled aliasing in PI results in higher acceleration (CAIPIRINHA, Siemens Healthcare) algorithm, which creates a shift between the two undersampling directions to improve image reconstruction quality, noise, and aliasing artifacts [17, 27] (Fig. 4). Two studies evaluated the performance of fully automated one-button-push 3D CAIPIRINHA SPACE TSE protocols for 10-minute acquisition of MRI examinations of the knee for children and adults [16, 18]. For pediatric patients, the 10-minute protocol resulted in surgically confirmed diagnostic accuracies of 84–100% for detecting articular cartilage defects, meniscus tears, and ligament injuries [17, 18]. For adults, the diagnostic performance of the 10-minute 3D MRI protocols for detecting internal derangement was interchangeable with that of the 20-minute 2D TSE standard-of-reference MRI protocols performed with field strengths of both 1.5 T and 3 T [16].

Simultaneous Multislice Acceleration

How It Works

SMS acceleration techniques acquire several images in a stack of MR images at the same time [28], whereas traditional pulse sequences acquire one image at a time. Dedicated deconvolution algorithms are used to separate the mixed MR signals from the originating slices, using coil sensitivity profiles, FOV shifts, and gradient encoding [27. Similar to PI acceleration, SMS acceleration requires the use of multichannel array coils [29]. SMS acceleration effectively reduces the total TR that is required to complete a pulse sequence [30], which can be translated into direct and indirect time savings.

Practical Considerations

In contrast to PI acceleration, SMS acceleration techniques sample all phase-encoding steps and are therefore almost SNR neutral. The number of simultaneously acquired slices equal the SMS acceleration factor, which reduces the acquisition time proportionally (see equation 1); however, reductions in acquisition time need to be realized through conversions of TR, echo-train length, or both.

In musculoskeletal MRI, indirect time savings result from SMS acceleration affording acquisition of twice the number of slices in a time-neutral fashion, which can be used to minimize or avoid slice gaps, increase anatomic coverage, or use thinner slices while keeping the anatomic coverage constant. Other solutions include the time-neutral use of techniques that consume TR, such as the use of spectral attenuated inversion recovery (SPAIR) for more homogeneous fat suppression (Table 5 and Fig. 6).

Direct time savings result from a numeric reduction of the TR, reducing the number of slice packages (i.e., concatenations) or increasing the echo-train length.

For musculoskeletal MRI protocols that use native and fat-suppressed T1-weighted pulse sequences, slice coverage often requires concatenation of slices to fit the short TR. SMS acceleration reduces the number of concatenations, which directly translates into time savings.

For musculoskeletal MRI protocols using PD-weighted and T2-weighted pulse sequences, sufficiently long TRs are important determinants of fluid sensitivity, high SNR gain, and contrast differentiation of musculoskeletal tissues. TR should only be reduced if it is greater than 3500–4000 ms, and SMS acceleration decreases the number of required concatenations and excess TR, resulting in a proportionate reduction in acquisition time.

Another strategy is to apply the benefits of SMS acceleration for longer echo trains. In scenarios in which the combination of echo spacing and TR permits limited echo-train length only, SMS acceleration enables longer echo trains, which are directly proportional to a shorter acquisition time.

In contrast to PI, SMS acceleration may result in higher specific absorption rate values because of the sum of simultaneously imparted radiofrequency pulses. However, dedicated radiofrequency pulse designs [31], flip angles of 125–150°, and local transmit coils can reduce the specific absorption rate to the level observed for conventional FSE and TSE pulse sequences.

Musculoskeletal Applications

SMS acceleration has been used for faster acquisition of MRI examinations of the hip [32]. When T1-weighted, PD-weighted, and fat-suppressed T2-weighted TSE sequences are used, SMS acceleration afforded a nearly SNR-neutral reduction in acquisition time of 38% compared with PI acceleration. SMS acceleration yielded lower numbers of signals and concatenations.

For knee MRI, SMS acceleration was successfully used as the sole technique for twofold acceleration [33]. The SMS acceleration protocol was 51% shorter than the unaccelerated version and included T1-weighted and fat-suppressed, PD-weighted TSE sequences. SNR, image contrast, and frequency of detecting abnormalities were similar between the two protocols.

For imaging of the spine, SMS acceleration was used instead of PI to achieve nearly SNR-neutral twofold acceleration of an axial T2-weighted TSE pulse sequence [34]. SMS acceleration contributed to a comprehensive spine protocol with a total acquisition time of 5–6 minutes.

TABLE 5: Comprehensive 5-Minute Protocol for 3-T MRI of the Knee With Combined Parallel Imaging (PI) and Simultaneous Multislice (SMS) Acceleration

Parameter	Axial PD-Weighted FS Image	Sagittal PD-Weighted Image	Sagittal T2-Weighted FS Image	Coronal PD-Weighted FS Image	Coronal T1-Weighted Image
Gradient performance	High	High	High	High	High
Radiofrequency speed	Fast	Fast	Fast	Fast	Fast
Fat suppression	SPAIR	—	SPAIR	SPAIR	—
TR (ms)	3600	3480	3700	3510	546
TE (ms)	32	23	56	35	7.1
Echo-train length	11	11	11	11	4
Bandwidth (Hz/pixel)	296	354	299	301	355
FOV (mm)	140 × 140	140 × 140	140 × 140	140 × 140	140 × 140
Matrix size	272 × 204	336 × 252	304 × 228	272 × 204	256 × 179
Slice thickness (mm)	3	3	3	3	3.5
No. of slices	38	38	38	36	28
PI acceleration factor	2	2	2	2	2
SMS acceleration factor	2	2	2	2	2
Phase direction	Right to left	Head to foot	Head to foot	Head to foot	Right to left
Phase oversampling (%)	38	39	83	94	12
Flip angle (°)	125	125	125	125	125
Echo spacing (ms)	7.1	7.5	8.0	7.1	7.1
Acquisition time	1 min 00 s	1 min 08 s	1 min 23 s	1 min 15 s	0 min 22 s

Note—Dash (—) denotes no fat suppression was used. PD = proton density, FS = fat suppressed, SPAIR = spectral attenuated inversion recovery (Siemens Healthineers).

For musculoskeletal MRI protocols, the synergistic combination of SMS acceleration and PI is especially beneficial because SMS acceleration is nearly SNR neutral but increases the specific absorption rate, whereas PI results in signal loss but a similar specific absorption rate. The multiplicative effects of the acceleration factors of SMS acquisition and PI acquisition permit fourfold and sixfold acceleration of 2D FSE and TSE MRI examination of the knee with different image contrasts and plane orientations [30]. Fourfold acceleration of FSE and TSE pulse sequences permits the design of a 5-minute knee MRI protocol that consists of five pulse sequences, different plane orientations, different contrast weightings, and homogeneous SPAIR fat suppression (Table 5 and Fig. 6).

In a knee MRI study performed in a pediatric population, fourfold SMS acquisition– and PI-accelerated, fat-suppressed, T2-weighted TSE pulse sequences were 41% faster than PI acceleration and showed no differences in image quality and diagnostic performance [35].

Compressed Sensing–Based Undersampling

How It Works

Similar to PI, CS acceleration reduces acquisition time by undersampling phase-encoding information. Although PI samples phase-encoding information in lines (Fig. 1), CS uses nonlinear undersampling patterns and recovers missing data during image reconstruction [36] (Fig. 7). Furthermore, use of CS techniques often resulted in disproportionate undersampling of areas with less dense or less critical information [37].

Practical Considerations

Recovery of missing data during image reconstruction is a practically relevant feature of CS that sets it apart from the lossier undersampling of PI [38, 39]. Depending on the acceleration factor, number of iterations, and the number of voxels, CS-based image reconstructions can require longer than PI-based image reconstructions. However, reductions in reconstruction times have been observed as software and workstation performances have evolved.

For musculoskeletal MRI, CS can be applied alone or in combination with PI to achieve higher accelerations, retain more SNR, and overcome geometric coil limitations that apply for PI. For 2D FSE and TSE sequences, the reported acceleration factors of PI, CS, and the combination of CS and PI are similar, ranging from 2 to 3 [6–10, 40, 41]; however, CS accelerations may retain more SNR [40, 41].

For 3D FSE and TSE sequences, CS can achieve faster acceleration than PI alone and can retain more SNR [42, 43]. For example, although PI can achieve twofold, threefold, and fourfold acceleration of 3D FSE and TSE pulse sequences [16, 18, 20, 25, 26], CS and combined PI and CS techniques can achieve fivefold and sixfold accelerations of 3D FSE and TSE sequences [42, 43]. Faster acceleration factors are afforded by the increased number of areas of sparse signal in 3D FSE and TSE pulse sequences for which CS undersampling achieves higher acceleration factors and gains in SNR than PI.

CS achieves substantially higher acceleration factors than PI when combined with advanced metal artifact reduction pulse sequences [44–46]. The high intrinsic sparsity renders SEMAC

and multiacquisition variable-resonance image combination (MAVRIC) metal artifact reduction pulse sequences [45, 47, 48] nearly ideally suitable for CS acceleration. Although PI acceleration is usually limited to a factor of 3 [46, 49, 50], CS enables acceleration factors of 8 [44, 46, 51]. With use of the combination of CS acceleration and elliptical scanning, SEMAC acquisition times can be reduced by 60–70% to 4–5 minutes per sequence (Fig. 8), which in some instances permits the time-neutral use of SEMAC compared with conventional high-bandwidth 2D FSE and TSE pulse sequences [52, 53].

Musculoskeletal Applications

The combination of PI and CS enabled two- and threefold acceleration of 2D knee MRI examinations when T1-weighted and fat-suppressed PD- and T2-weighted 2D FSE pulse sequences were obtained at a field strength of 3 T. When compared with unaccelerated 2D FSE and TSE, twofold and threefold accelerations were reported to afford acquisition times that are 40% and 59% faster, respectively, providing similar image quality but limited interreader agreements [40].

A study evaluating 3-T MRI examination of the ankle compared twofold acceleration using PI and 2.5-fold acceleration using the combination of PI and CS for T1-weighted, fat-suppressed PD-weighted, and T2-weighted 2D TSE pulse sequences [41]. Acceleration with the combination of CS and PI was 18% faster than that with PI alone and yielded similar visibility of anatomic structures as well as similar SNR and contrast-to-noise ratio in musculoskeletal structures.

CS applied to 3D knee MRI afforded sixfold accelerations of isotropic intermediate-weighted and fat-suppressed T2-weighted 3D SPACE TSE datasets (Fig. 9) with an isotropic voxel size of 0.5–0.6 mm^3 and an acquisition time of 5 minutes per sequence [42]. Compared with twofold accelerated conventional 3D SPACE TSE MRI, CS afforded an acquisition time that was 60% faster. The diagnostic performance of a 10-minute CS-accelerated 3D SPACE protocol was similar to that of a 20-minute 2D TSE reference standard MRI protocol for detecting internal derangement.

In another study that evaluated fast 3D knee MRI, CS acceleration reduced the acquisition time for an isotropic, fat-suppressed, PD-weighted 3D SPACE TSE pulse sequence from 7 minutes 28 seconds to 5 minutes [54]. Cartilage lesions, high signal intensity of synovial fluid, and menisci were best visualized on CS SPACE images, whereas 2D TSE images showed bones, ligaments, muscles, and fat to better advantage.

CS acceleration of a fat-suppressed PD-weighted 3D Cube (GE Healthcare) FSE sequence with an anisotropic voxel size of 0.5 × 0.5 × 1.0 mm resulted in a 31% reduction in acquisition time from 4 minutes 44 seconds to 3 minutes 16 seconds [43]. PI-accelerated and CS-accelerated Cube FSE sequences had similar performance in diagnosing internal derangement.

Acceleration achieved using a combination of CS and PI with zero-filling interpolation of an anisotropic axial PD-weighted 3D Cube FSE pulse sequence reduced the acquisition time of 3D MRI examinations of the shoulder from 3 minutes 32 seconds to 2 minutes 22 seconds [55]. Structural similarity indexes and frequency of detection of abnormalities were similar for both pulse sequences.

Multiple studies have described the clinical application of eightfold accelerated STIR, T1-weighted, PD-weighted, and T2-weighted SEMAC pulse sequences for metal artifact reduction MRI examinations in patients with hip [51, 56–58], knee [44], and ankle [59, 60] arthroplasty implants, achieving 60–70% reductions in acquisition times when compared with PI-accelerated protocols.

Use of multispectral imaging pulse sequences accelerated by the combination of PI and CS for imaging of the spine has been described elsewhere [45]. Acceleration factors of 5.2–6 reduced the acquisition time of a T2-weighted multispectral imaging pulse sequence from 9 to 10 minutes to 7 to 8 minutes and produced similar structural similarity indexes and observer-rated image quality.

Synthetic MRI

How It Works

Synthetic MRI describes techniques that use quantitative T1, PD, and T2 maps to calculate morphologic MR images with postprocessing software rather than sample the information of morphologic MR images [61]. During postprocessing, the operator can choose any TR, any TE, and different inversion times for final MR images along with virtually unlimited numbers of contrasts.

For musculoskeletal MRI, synthetic MRI can achieve savings in acquisition time through the simultaneous generation of quantitative maps and morphologic MR images, which would otherwise require longer, separate acquisitions.

Practical Considerations

In addition to classic T1-weighted, PD-weighted, T2-weighted, and STIR MR images, new contrasts can be generated from the quantitative parental dataset, such as fat- and fluid-suppressed MR images used as a surrogate for contrast-enhanced, fat-suppressed, T1-weighted MR images [62].

Fat can be suppressed during postprocessing with synthetic STIR techniques, or the parental synthetic MRI dataset can be acquired with spectral fat suppression [63, 64]. With use of the latter technique, however, only fat-suppressed morphologic MR images can be generated synthetically.

At present, most synthetic techniques use 2D pulse sequences, which limit synthetic MR images to the acquired plane; however, 3D acquisitions that permit multiplanar reformatted MR images are under investigation [65].

Synthetic MRI can be realized in various ways. A combination of pulse sequences that obtain quantitative T1, PD, and T2 data permits synthesis of the full spectrum of musculoskeletal contrasts with any combination of short and long TRs and TEs, respectively, in addition to added inversion times [61, 66] (Fig. 10). The use of a quantitative pulse sequence that maps the T2 spectrum only will limit synthesizing morphologic MR images to long TR contrasts, including PD- and T2-weighted MR images [64, 67, 68].

Musculoskeletal Applications

Full-spectrum synthetic 3-T MRI examination of the knee performed using a 10-minute synthetic protocol can generate accurate quantitative T1, PD, and T2 maps as well as morphologic T1-weighted, PD-weighted, T2-weighted, and STIR MR images [61]. Synthetic and conventionally acquired MR images had similar image quality and diagnostic performance. The efficiency gain of synthetic MRI was the time-neutral acquisition of quantitative maps.

T2-spectrum synthetic 3-T MRI examination of the knee performed using a 7-minute synthetic MRI protocol with spectral fat suppression is feasible for generating accurate quantitative T2 maps and morphologic fat-suppressed PD- and T2-weighted MR images [64]. Synthetic and conventionally acquired MR images had similar interreader agreements for diagnosing internal derangement, whereas synthetic MRI afforded time-neutral acquisition of accurate T2 maps.

In a study that investigated the clinical utility of full-spectrum synthetic MRI of the knee performed at a field strength of 1.5 T found that synthetic MR images acquired using a 7-minute protocol can replace conventionally acquired T1-weighted, PD-weighted, and STIR MR images obtained using a 12-minute clinical MRI protocol for the diagnosis of a variety of knee conditions [69].

In a study evaluating diagnosis of knee synovitis with 3-T MRI, a 6-minute, full-spectrum, synthetic MRI protocol was used to generate classic musculoskeletal contrast MR images and, in addition, MR images with combined water and fat suppression as a replacement for gadolinium contrast medium–enhanced, fat-suppressed, T1-weighted MR images [70]. With allowance for some limitations, synthetic water and fat suppression MR images were capable of diagnosing knee synovitis, representing a promising alternative for use in scenarios in which gadolinium administration is not feasible.

In a study investigating the utility of full-spectrum synthetic MRI for MR arthrography examinations of the shoulder [71], coronal oblique synthetic pulse sequences had a faster acquisition time (6 minutes 20 seconds) than did images obtained using the conventional protocol. For synthetic T1-weighted MR images, postprocessing permitted identification of optimal TRs and TEs to allow maximization of the contrast between gadolinium-enhanced joint fluid and the labrum, and for T2-weighted MR images, it allowed maximization of the contrast between fluid and rotator cuff tendons. The individual adjustments improved the conspicuity of labral and rotator cuff lesions.

In a study focusing on characterization of articular cartilage of the knee, a fat-suppressed, double-echo, steady-state pulse sequence was used to synthesize T2 maps in addition to morphologic MR images, permitting segmentation, quantification, and structural evaluation of articular cartilage [72]. The efficiency gain was the near time-neutral acquisition of T2 maps in a total sequence acquisition time of 5 minutes or less.

Combined Use of Advanced Acceleration Techniques

The advanced acceleration technique can be applied to pulse sequences that previously were optimized using widely accessible techniques [1]. The advanced techniques can be combined in practice, which leads to synergies through the multiplication of acceleration factors, SNR gains, and specific absorption rate. Table 6 provides a checklist for applying the different acceleration techniques to the spectrum of FSE and TSE pulse sequences.

Conclusion

Advanced acceleration techniques, including PI, SMS acceleration, CS, and synthetic MRI techniques, provide unprecedented opportunities for rapid musculoskeletal MRI examinations while retaining quality, comprehensiveness, and diagnostic performance. The combined use of advanced acceleration techniques is advantageous for rapid musculoskeletal MRI examinations: combined PI and SMS acceleration enables fourfold to sixfold accelerations of 2D FSE and TSE pulse sequences, combined use of PI and CS enables fourfold to sixfold accelerations of 3D FSE and TSE pulse sequences, and combined CS and elliptical scanning enables fivefold to eightfold accelerations of advanced metal artifact reduction pulse sequences. Synthetic MRI techniques permit the time-neutral acquisition of quantitative maps and the generation of virtually unlimited musculoskeletal MRI contrasts. Acceleration factors of 3–8 can be realized in clinical practice, amounting to time savings of 65–85% compared with unaccelerated acquisitions.

TABLE 6: Checklist of Advanced Techniques for Rapid Musculoskeletal MRI

Technique	Effect on Acquisition Time	Musculoskeletal Applications
Parallel imaging acceleration	Acquisition time decreases proportionally to the acceleration factor	Twofold to threefold acceleration of 2D FSE and TSE pulse sequences
		Fourfold acceleration of 3D FSE and TSE pulse sequences
SMS acceleration	Acquisition time decreases through shorter minimum TR, fewer concatenations, and longer possible echo trains	Near SNR-neutral twofold and threefold acceleration of 2D FSE and TSE pulse sequences
		Combined fourfold to sixfold SMS and parallel imaging acceleration of 2D FSE and TSE pulse sequences
Compressed sensing acceleration	Acquisition time decreases proportionally to the acceleration factor; may afford faster acceleration and less SNR loss than parallel imaging	Fivefold to sixfold acceleration of 3D FSE and TSE pulse sequences
		Fivefold to eightfold acceleration of SEMAC and multispectral imaging pulse sequences
Synthetic MRI	Time-neutral acquisition of quantitative maps and creations of multiple musculoskeletal contrasts	Quantitative mapping in time-neutral fashion
		Limitless creation of classic and new MRI contrasts

Note—FSE = fast spin-echo, TSE = turbo spin-echo, SMS = simultaneous multislice, SEMAC = slice encoding for metal artifact correction, SNR = signal-to-noise ratio.

References

1. Del Grande F, Guggenberger R, Fritz J. Rapid musculoskeletal MRI in 2020: value and optimized use of widely accessible techniques. *AJR* 2020 (in press)
2. Deshmane A, Gulani V, Griswold MA, Seiberlich N. Parallel MR imaging. *J Magn Reson Imaging* 2012; 36:55–72
3. Pruessmann KP, Weiger M, Scheidegger MB, Boesiger P. SENSE: sensitivity encoding for fast MRI. *Magn Reson Med* 1999; 42:952–962
4. Griswold MA, Jakob PM, Heidemann RM, et al. Generalized autocalibrating partially parallel acquisitions (GRAPPA). *Magn Reson Med* 2002; 47:1202–1210
5. Blaimer M, Breuer F, Mueller M, Heidemann RM, Griswold MA, Jakob PM. SMASH, SENSE, PILS, GRAPPA: how to choose the optimal method. *Top Magn Reson Imaging* 2004; 15:223–236
6. Schnaiter JW, Roemer F, McKenna-Kuettner A, et al. Diagnostic accuracy of an MRI protocol of the knee accelerated through parallel imaging in correlation to arthroscopy. *RoFo Fortschr Geb Rontgenstr Nuklearmed* 2018; 190:265–272
7. Magee T, Shapiro M, Williams D. Usefulness of simultaneous acquisition of spatial harmonics technique for MRI of the knee. *AJR* 2004; 182:1411–1415
8. Magee T, Shapiro M, Williams D, Ramnath RR, Simon J. Usefulness of the simultaneous acquisition of spatial harmonics technique during MRI of the shoulder. *AJR* 2003; 181:961–964
9. Subhas N, Benedick A, Obuchowski NA, et al. Comparison of a fast 5-minute shoulder MRI protocol with a standard shoulder MRI protocol: a multi-institutional multireader study. *AJR* 2017; 208:[web]W146–W154
10. Alaia EF, Benedick A, Obuchowski NA, et al. Comparison of a fast 5-min knee MRI protocol with a standard knee MRI protocol: a multi-institutional multi-reader study. *Skeletal Radiol* 2018; 47:107–116
11. Van Dyck P, Kenis C, Vanhoenacker FM, et al. Comparison of 1.5- and 3-T MR imaging for evaluating the articular cartilage of the knee. *Knee Surg Sports Traumatol Arthrosc* 2014; 22:1376–1384
12. Van Dyck P, Vanhoenacker FM, Lambrecht V, et al. Prospective comparison of 1.5 and 3.0-T MRI for evaluating the knee menisci and ACL. *J Bone Joint Surg Am* 2013; 95:916–924
13. Sutter R, Ulbrich EJ, Jellus V, Nittka M, Pfirrmann CW. Reduction of metal artifacts in patients with total hip arthroplasty with slice-encoding metal artifact correction and view-angle tilting MR imaging. *Radiology* 2012; 265:204–214
14. Sutter R, Hodek R, Fucentese SF, Nittka M, Pfirrmann CW. Total knee arthroplasty MRI featuring slice-encoding for metal artifact correction: reduction of artifacts for STIR and proton density-weighted sequences. *AJR* 2013; 201:1315–1324
15. Mugler JP 3rd. Optimized three-dimensional fast-spin-echo MRI. *J Magn Reson Imaging* 2014; 39:745–767
16. Del Grande F, Delcogliano M, Guglielmi R, et al. Fully automated 10-minute 3D CAIPIRINHA SPACE TSE MRI of the knee in adults: a multicenter, multireader, multifield-strength validation study. *Invest Radiol* 2018; 53:689–697
17. Fritz J, Fritz B, Thawait GG, Meyer H, Gilson WD, Raithel E. Three-dimensional CAIPIRINHA SPACE TSE for 5-minute high-resolution MRI of the knee. *Invest Radiol* 2016; 51:609–617
18. Fritz J, Ahlawat S, Fritz B, et al. 10-Min 3D turbo spin echo MRI of the knee in children: arthroscopy-validated accuracy for the diagnosis of internal derangement. *J Magn Reson Imaging* 2019; 49:e139–e151
19. Fritz B, Bensler S, Thawait GK, Raithel E, Stern SE, Fritz J. CAIPIRINHA-accelerated 10-min 3D TSE MRI of the ankle for the diagnosis of painful ankle conditions: performance evaluation in 70 patients. *Eur Radiol* 2019; 29:609–619
20. Kalia V, Fritz B, Johnson R, Gilson WD, Raithel E, Fritz J. CAIPIRINHA accelerated SPACE enables 10-min isotropic 3D TSE MRI of the ankle for optimized visualization of curved and oblique ligaments and tendons. *Eur Radiol* 2017; 27:3652–3661
21. Shakoor D, Guermazi A, Kijowski R, et al. Cruciate ligament injuries of the knee: a meta-analysis of the diagnostic performance of 3D MRI. *J Magn Reson Imaging* 2019; 50:1545–1560
22. Shakoor D, Guermazi A, Kijowski R, et al. Diagnostic performance of three-dimensional MRI for depicting cartilage defects in the knee: a meta-analysis. *Radiology* 2018; 289:71–82
23. Shakoor D, Kijowski R, Guermazi A, et al. Diagnosis of knee meniscal injuries by using three-dimensional MRI: s systematic review and meta-analysis of diagnostic performance. *Radiology* 2019; 290:435–445
24. Jung JY, Yoon YC, Choi SH, Kwon JW, Yoo J, Choe BK. Three-dimensional isotropic shoulder MR arthrography: comparison with two-dimensional MR arthrography for the diagnosis of labral lesions at 3.0 T. *Radiology* 2009; 250:498–505
25. Notohamiprodjo M, Horng A, Kuschel B, et al. 3D-imaging of the knee with an optimized 3D-FSE-sequence and a 15-channel knee-coil. *Eur J Radiol* 2012; 81:3441–3449
26. Kijowski R, Davis KW, Woods MA, et al. Knee joint: comprehensive assessment with 3D isotropic resolution fast spin-echo MR imaging: diagnostic performance compared with that of conventional MR imaging at 3.0 T. *Radiology* 2009; 252:486–495
27. Breuer FA, Blaimer M, Mueller MF, et al. Controlled aliasing in volumetric parallel imaging (2D CAIPIRINHA). *Magn Reson Med* 2006; 55:549–556
28. Larkman DJ, Hajnal JV, Herlihy AH, Coutts GA, Young IR, Ehnholm G. Use of multicoil arrays for separation of signal from multiple slices simultaneously excited. *J Magn Reson Imaging* 2001; 13:313–317
29. Barth M, Breuer F, Koopmans PJ, Norris DG, Poser BA. Simultaneous multislice (SMS) imaging techniques. *Magn Reson Med* 2016; 75:63–81
30. Fritz J, Fritz B, Zhang J, et al. Simultaneous multislice accelerated turbo spin echo magnetic resonance imaging: comparison and combination with in-plane parallel imaging acceleration for high-resolution magnetic resonance imaging of the knee. *Invest Radiol* 2017; 52:529–537
31. Hargreaves BA, Cunningham CH, Nishimura DG, Conolly SM. Variable-rate selective excitation for rapid MRI sequences. *Magn Reson Med* 2004; 52:590–597
32. Haraikawa M, Suzuki M, Inoue K, Kozawa E, Tanaka J, Niitsu M. Simultaneous multi-slice MR imaging of the hip at 3cT to reduce acquisition times and maintain image quality. *BMC Musculoskelet Disord* 2018; 19:440
33. Li X, Peng Z, Sun Y, Cui J. Is simultaneous multisection turbo spin echo ready for clinical MRI? A feasibility study on fast imaging of knee lesions. *Clin Radiol* 2020; 75(3):238.e21–238.e30
34. Longo MG, Fagundes J, Huang S, et al. Simultaneous multislice-based 5-minute lumbar spine MRI protocol: initial experience in a clinical setting. *J Neuroimaging* 2017; 27:442–446
35. Benali S, Johnston PR, Gholipour A, et al. Simultaneous multi-slice accelerated turbo spin echo of the knee in pediatric patients. *Skeletal Radiol* 2018; 47:821–831
36. Lustig M, Donoho D, Pauly JM. Sparse MRI: The application of compressed sensing for rapid MR imaging. *Magn Reson Med* 2007; 58:1182–1195
37. Li G, Zaitsev M, Büchert M, et al. Improving the robustness of 3D turbo spin echo imaging to involuntary motion. *MAGMA* 2015; 28:329–345
38. Feng L, Benkert T, Block KT, Sodickson DK, Otazo R, Chandarana H. Compressed sensing for body MRI. *J Magn Reson Imaging* 2017; 45:966–987
39. Geethanath S, Reddy R, Konar AS, et al. Compressed sensing MRI: a review. *Crit Rev Biomed Eng* 2013; 41:183–204
40. Matcuk GR, Gross JS, Fields BKK, Cen S. Compressed sensing MR imaging (CS-MRI) of the knee: assessment of quality, inter-reader agreement, and acquisition time. *Magn Reson Med Sci* 2020; 254–258

41. Gersing AS, Bodden J, Neumann J, et al. Accelerating anatomical 2D turbo spin echo imaging of the ankle using compressed sensing. *Eur J Radiol* 2019; 118:277–284
42. Fritz J, Raithel E, Thawait GK, Gilson W, Papp DF. Six-fold acceleration of high-spatial resolution 3D SPACE MRI of the knee through incoherent k-space undersampling and iterative reconstruction: first experience. *Invest Radiol* 2016; 51:400–409
43. Kijowski R, Rosas H, Samsonov A, King K, Peters R, Liu F. Knee imaging: rapid three-dimensional fast spin-echo using compressed sensing. *J Magn Reson Imaging* 2017; 45:1712–1722
44. Fritz J, Ahlawat S, Demehri S, et al. Compressed sensing SEMAC: 8-fold accelerated high resolution metal artifact reduction MRI of cobalt-chromium knee arthroplasty implants. *Invest Radiol* 2016; 51:666–676
45. Worters PW, Sung K, Stevens KJ, Koch KM, Hargreaves BA. Compressed-sensing multispectral imaging of the postoperative spine. *J Magn Reson Imaging* 2013; 37:243–248
46. Otazo R, Nittka M, Bruno M, et al. Sparse-SEMAC: rapid and improved SEMAC metal implant imaging using SPARSE-SENSE acceleration. *Magn Reson Med* 2017; 78:79–87
47. Lu W, Pauly KB, Gold GE, Pauly JM, Hargreaves BA. SEMAC: slice encoding for metal artifact correction in MRI. *Magn Reson Med* 2009; 62:66–76
48. Koch KM, Lorbiecki JE, Hinks RS, King KF. A multispectral three-dimensional acquisition technique for imaging near metal implants. *Magn Reson Med* 2009; 61:381–390
49. Fritz J, Lurie B, Miller TT. Imaging of hip arthroplasty. *Semin Musculoskelet Radiol* 2013; 17:316–327
50. Khodarahmi I, Isaac A, Fishman EK, Dalili D, Fritz J. Metal about the hip and artifact reduction techniques: from basic concepts to advanced imaging. *Semin Musculoskelet Radiol* 2019; 23:e68–e81
51. Fritz J, Fritz B, Thawait GK, et al. Advanced metal artifact reduction MRI of metal-on-metal hip resurfacing arthroplasty implants: compressed sensing acceleration enables the time-neutral use of SEMAC. *Skeletal Radiol* 2016; 45:1345–1356
52. Khodarahmi I, Haroun RR, Lee M, et al. Metal artifact reduction computed tomography of arthroplasty implants: effects of combined modeled iterative reconstruction and dual-energy virtual monoenergetic extrapolation at higher photon energies. *Invest Radiol* 2018; 53:728–735
53. Khodarahmi I, Fritz J. Advanced MR imaging after total hip arthroplasty: the clinical impact. *Semin Musculoskelet Radiol* 2017; 21:616–629
54. Altahawi FF, Blount KJ, Morley NP, Raithel E, Omar IM. Comparing an accelerated 3D fast spin-echo sequence (CS-SPACE) for knee 3-T magnetic resonance imaging with traditional 3D fast spin-echo (SPACE) and routine 2D sequences. *Skeletal Radiol* 2017; 46:7–15
55. Lee SH, Lee YH, Song HT, Suh JS. Rapid acquisition of magnetic resonance imaging of the shoulder using three-dimensional fast spin echo sequence with compressed sensing. *Magn Reson Imaging* 2017; 42:152–157
56. Jungmann PM, Bensler S, Zingg P, Fritz B, Pfirrmann CW, Sutter R. Improved visualization of juxtaprosthetic tissue using metal artifact reduction magnetic resonance imaging: experimental and clinical optimization of compressed sensing SEMAC. *Invest Radiol* 2019; 54:23–31
57. Galley J, Sutter R, Stern C, Filli L, Rahm S, Pfirrmann CWA. Diagnosis of periprosthetic hip joint infection using MRI with metal artifact reduction at 1.5 T. *Radiology* 2020; 296:98–108
58. Filli L, Jungmann PM, Zingg PO, et al. MRI with state-of-the-art metal artifact reduction after total hip arthroplasty: periprosthetic findings in asymptomatic and symptomatic patients. *Eur Radiol* 2020; 30:2241–2252
59. de Cesar Netto C, Schon LC, da Fonseca LF, Chinanuvathana A, Stern SE, Fritz J. Metal artifact reduction MRI for total ankle replacement sagittal balance evaluation. *Foot Ankle Surg* 2019; 25:739–747
60. de Cesar Netto C, Fonseca LF, Fritz B, et al. Metal artifact reduction MRI of total ankle arthroplasty implants. *Eur Radiol* 2018; 28:2216–2227
61. Kumar NM, Fritz B, Stern SE, Warntjes JBM, Lisa Chuah YM, Fritz J. Synthetic MRI of the knee: phantom validation and comparison with conventional MRI. *Radiology* 2018; 289:465–477
62. Yoo HJ, Hong SH, Oh HY, et al. Diagnostic accuracy of a fluid-attenuated inversion-recovery sequence with fat suppression for assessment of peripatellar synovitis: preliminary results and comparison with contrast-enhanced MR imaging. *Radiology* 2017; 283:769–778
63. Fritz J. T2 mapping without additional scan time using synthetic knee MRI. *Radiology* 2019; 293:631–632
64. Roux M, Hilbert T, Hussami M, Becce F, Kober T, Omoumi P. MRI T2 mapping of the knee providing synthetic morphologic images: comparison to conventional turbo spin-echo MRI. *Radiology* 2019; 293:620–630
65. Fujita S, Hagiwara A, Hori M, et al. Three-dimensional high-resolution simultaneous quantitative mapping of the whole brain with 3D-QALAS: an accuracy and repeatability study. *Magn Reson Imaging* 2019; 63:235–243
66. Vargas MI, Drake-Pérez M, Delattre BMA, Boto J, Lovblad KO, Boudabous S. Feasibility of a synthetic MR imaging sequence for spine imaging. *AJNR* 2018; 39:1756–1763
67. Hilbert T, Sumpf TJ, Weiland E, et al. Accelerated T_2 mapping combining parallel MRI and model-based reconstruction: GRAPPATINI. *J Magn Reson Imaging* 2018; 48:359–368
68. Tamir JI, Taviani V, Alley MT, et al. Targeted rapid knee MRI exam using T_2 shuffling. *J Magn Reson Imaging* 2019; 49:e195–e204
69. Boudabbous S, Neroladaki A, Bagetakos I, Hamard M, Delattre BM, Vargas MI. Feasibility of synthetic MRI in knee imaging in routine practice. *Acta Radiol Open* 2018; 7:2058460118769686
70. Yi J, Lee YH, Song HT, Suh JS. Double-inversion recovery with synthetic magnetic resonance: a pilot study for assessing synovitis of the knee joint compared to contrast-enhanced magnetic resonance imaging. *Eur Radiol* 2019; 29:2573–2580
71. Lee SH, Lee YH, Hahn S, Yang J, Song HT, Suh JS. Optimization of T2-weighted imaging for shoulder magnetic resonance arthrography by synthetic magnetic resonance imaging. *Acta Radiol* 2018; 59:959–965
72. Chaudhari AS, Stevens KJ, Sveinsson B, et al. Combined 5-minute double-echo in steady-state with separated echoes and 2-minute proton-density-weighted 2D FSE sequence for comprehensive whole-joint knee MRI assessment. *J Magn Reson Imaging* 2019; 49:e183–e194

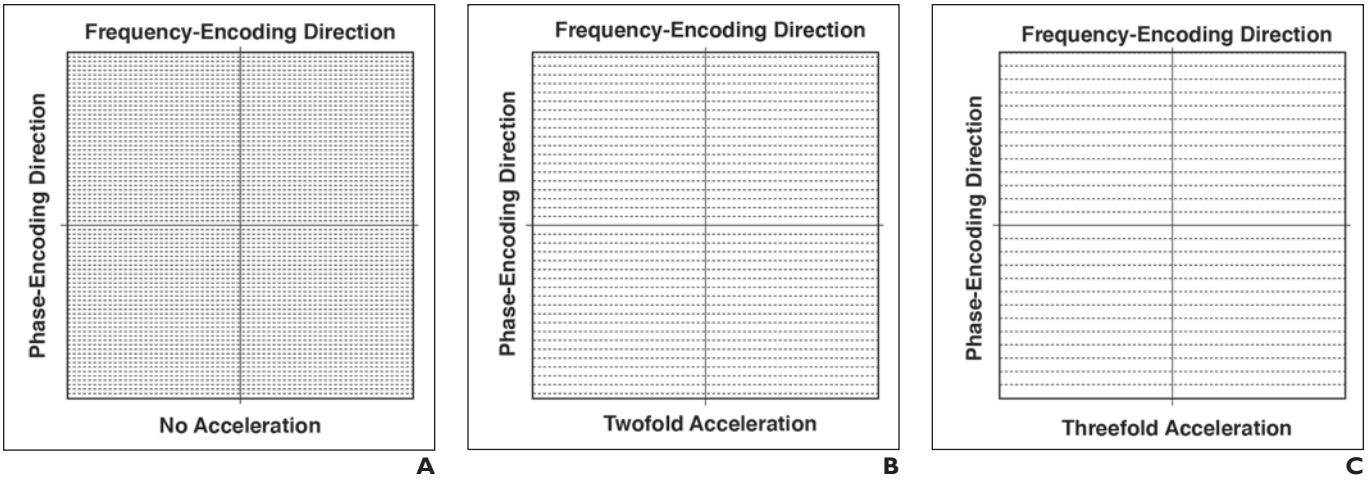

Fig. 1—Parallel imaging acceleration of 2D fast spin-echo and turbo spin-echo pulse sequences.
A–**C,** Schematics show fully sampled phase-encoding information (**A**), twofold parallel imaging acceleration achieved through sampling of every second phase-encoding step only (**B**), and threefold parallel imaging acceleration achieved through sampling of every third phase-encoding step only (**C**). Dotted horizontal lines indicate signal sampling lines in case space.

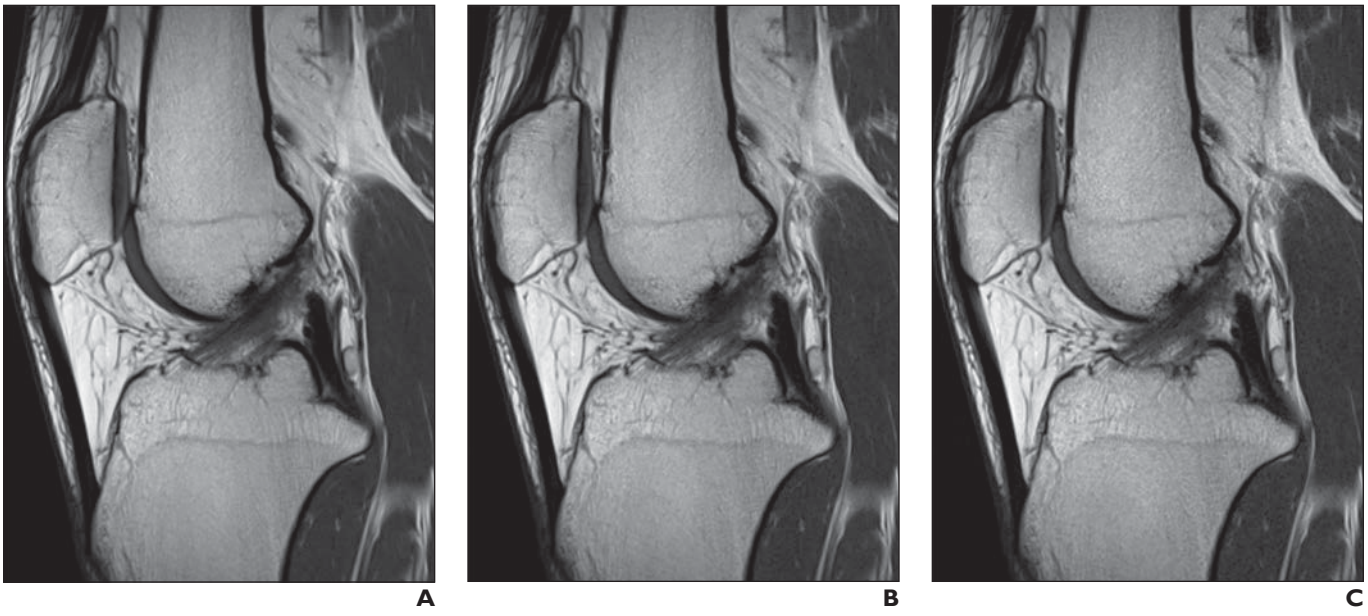

Fig. 2—32-year-old healthy man. Parallel imaging GRAPPA (Siemens Healthcare) acceleration of sagittal proton density–weighted musculoskeletal MR images acquired using 3-T MRI system, 15-channel knee coil, and pulse sequence parameters as shown in Table 1. GRAPPA enables artifact-free acceleration factors of up to 3 with decreasing acquisition times and signal-to-noise ratios. For this 15-channel knee coil configuration consisting of three rings in head-to-foot direction, each with five elements, parallel imaging acceleration is limited to factor of 3 in head-to-foot direction.
A–**C,** Appearance of MR images obtained using no acceleration (acquisition time, 3 minutes 50 seconds) (**A**), GRAPPA factor 2 acceleration (acquisition time, 2 minutes 2 seconds) (**B**), and GRAPPA factor 3 acceleration (acquisition time, 2 minutes 2 seconds) (**C**).

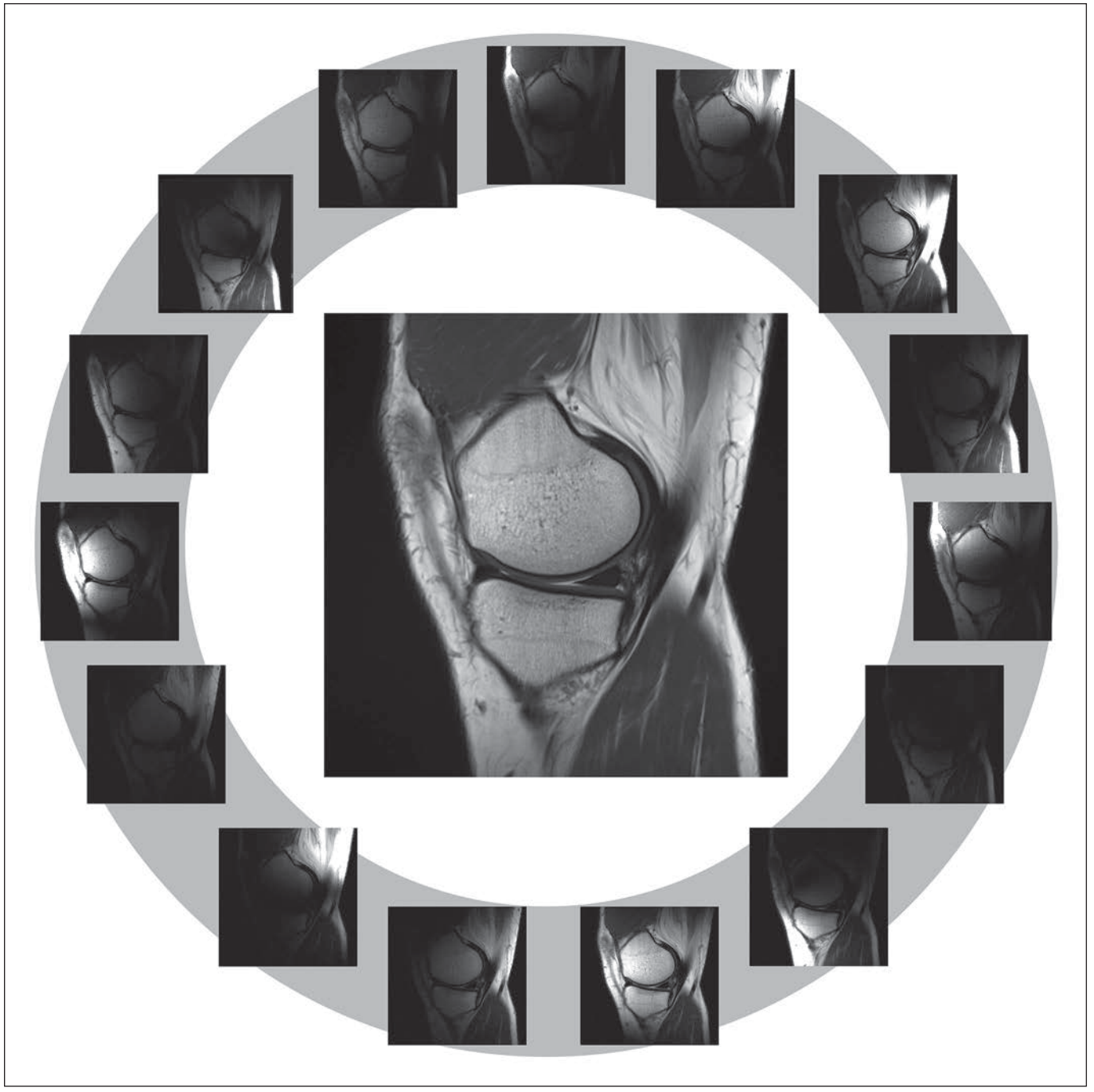

Fig. 3—32-year-old healthy man.Parallel imaging acquisition of knee performed using 15-channel receiver array coil (denoted by *gray circle*). Each of 15 coil elements obtains partial image (denoted by *images* along *gray circle*) on basis of location and distance to anatomic region, which allows spatial allocation of origin of received data for construction of final composite MR image (*center image*).

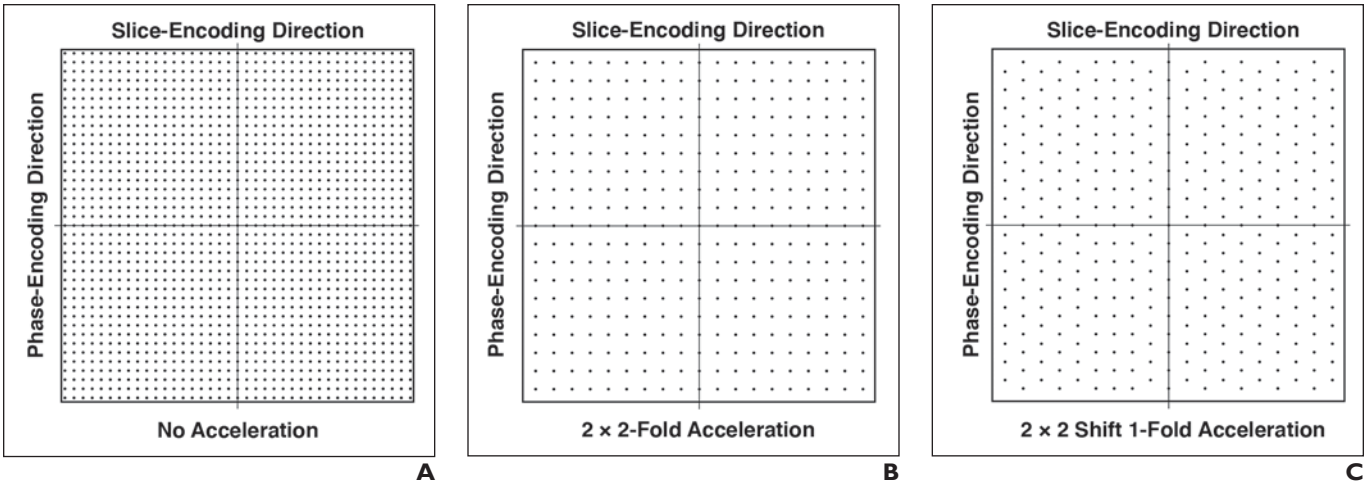

Fig. 4—Parallel imaging acceleration of 3D fast spin-echo and turbo spin-echo pulse sequences.
A–**C,** Schematics show fully sampled phase-encoding information (**A**); combined fourfold parallel imaging acceleration achieved through sampling of every second phase-encoding step in phase and slice (partition) directions, respectively (**B**); and combined fourfold parallel imaging acceleration with controlled aliasing in parallel imaging results in higher acceleration (CAIPIRINHA) algorithm introducing additional shift between skipped phase- and slice-encoding steps (**C**). Dotted horizontal lines indicate signal sampling lines in case space.

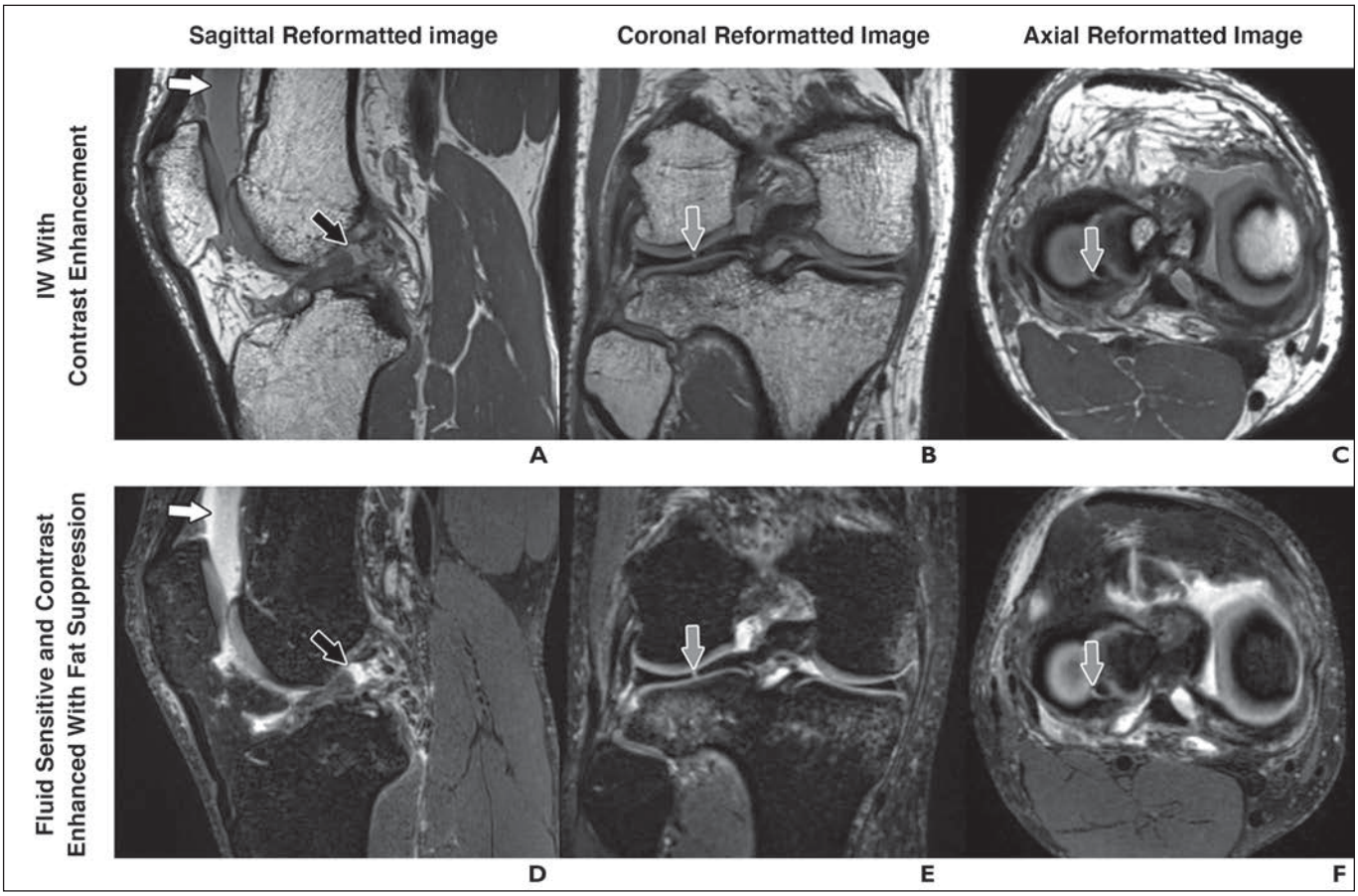

Fig. 5—30-year-old man with acute knee trauma who underwent 10-minute isotropic 3D CAIPIRINHA (controlled aliasing in parallel imaging results in higher acceleration, Siemens Healthcare) SPACE turbo spin-echo 3-T MRI examination of knee performed with use of 15-channel knee coil and pulse sequence parameters as shown in Table 3. Acquisition time of each 3D CAIPIRINHA SPACE turbo spin-echo pulse sequence was 5 minutes or less, whereas acquisition times for sequences obtained without acceleration and with twofold acceleration were more than 20 minutes and more than 10 minutes per sequence, respectively.
A–**F,** Intermediate-weighted (IW) (spatial resolution, 0.5 × 0.5 × 0.5 mm), unenhanced sagittal (**A**), coronal (**B**), and axial (**C**) MR reformatted images and fluid-sensitive (spatial resolution, 0.6 × 0.6 × 0.6 mm), unenhanced, fat-suppressed sagittal (**D**), coronal (**E**), and axial (**F**) MR reformatted images show full-thickness tear of anterior cruciate ligament (*black arrows*, **A** and **D**), parrot beak tear of lateral meniscus (*arrows*, **B, C, E**, and **F**), and hemorrhagic joint effusion with fluid-fluid level (*white arrows*, **A** and **D**).

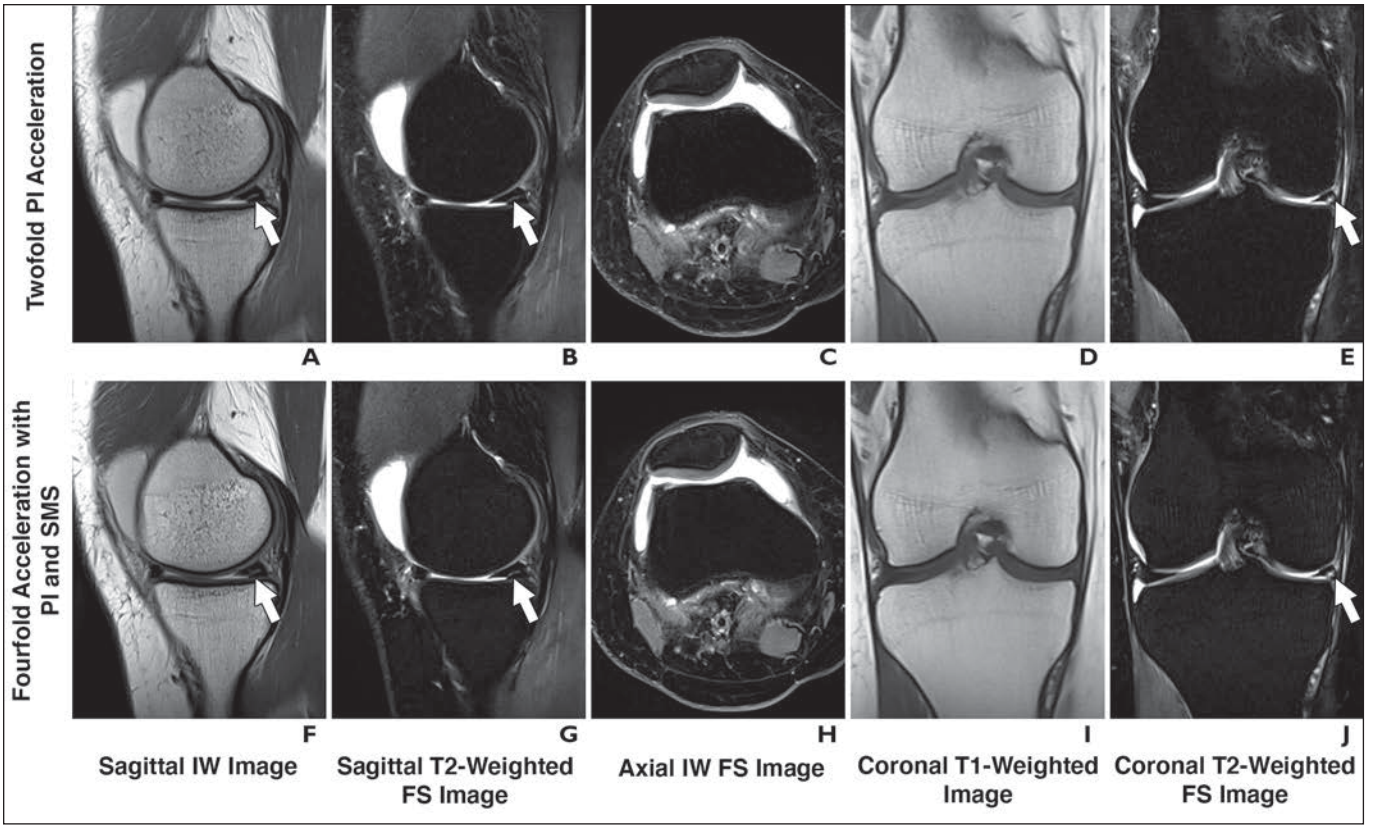

Fig. 6—45-year-old man with acute knee trauma who underwent MRI examination performed using combined parallel imaging (PI) and simultaneous multislice (SMS) acceleration with use of 3-T MRI system and 15-channel knee coil. IW = intermediate-weighted, FS = fat-suppressed.
A–**E,** Twofold PI-accelerated turbo spin-echo pulse sequences with total acquisition time of 9 minutes show moderate-to-large knee joint effusion and complex partial-thickness medial meniscus tear (*arrows*, **A**, **B**, and **E**)
F–**J,** Fourfold SMS- and PI-accelerated turbo spin-echo pulse sequences with total acquisition time of 5 minutes show moderate-to-large knee joint effusion and complex partial-thickness medial meniscus tear (*arrows*, **F**, **G**, and **J**)

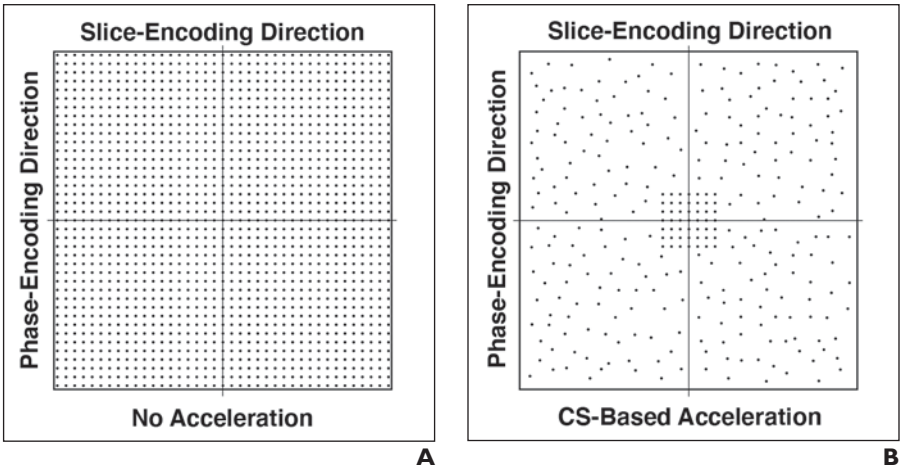

Fig. 7—Compressed sensing (CS)-based acceleration of 3D fast spin-echo and turbo spin-echo pulse sequences.
A and **B,** Schematics (k-space) show fully sampled phase-encoding information (**A**) and CS-based sampling pattern (**B**) with pseudorandom undersampling of peripheral phase-encoding information and full sampling shown centrally (*square*, **B**). Dotted horizontal lines indicate signal sampling lines in case space.

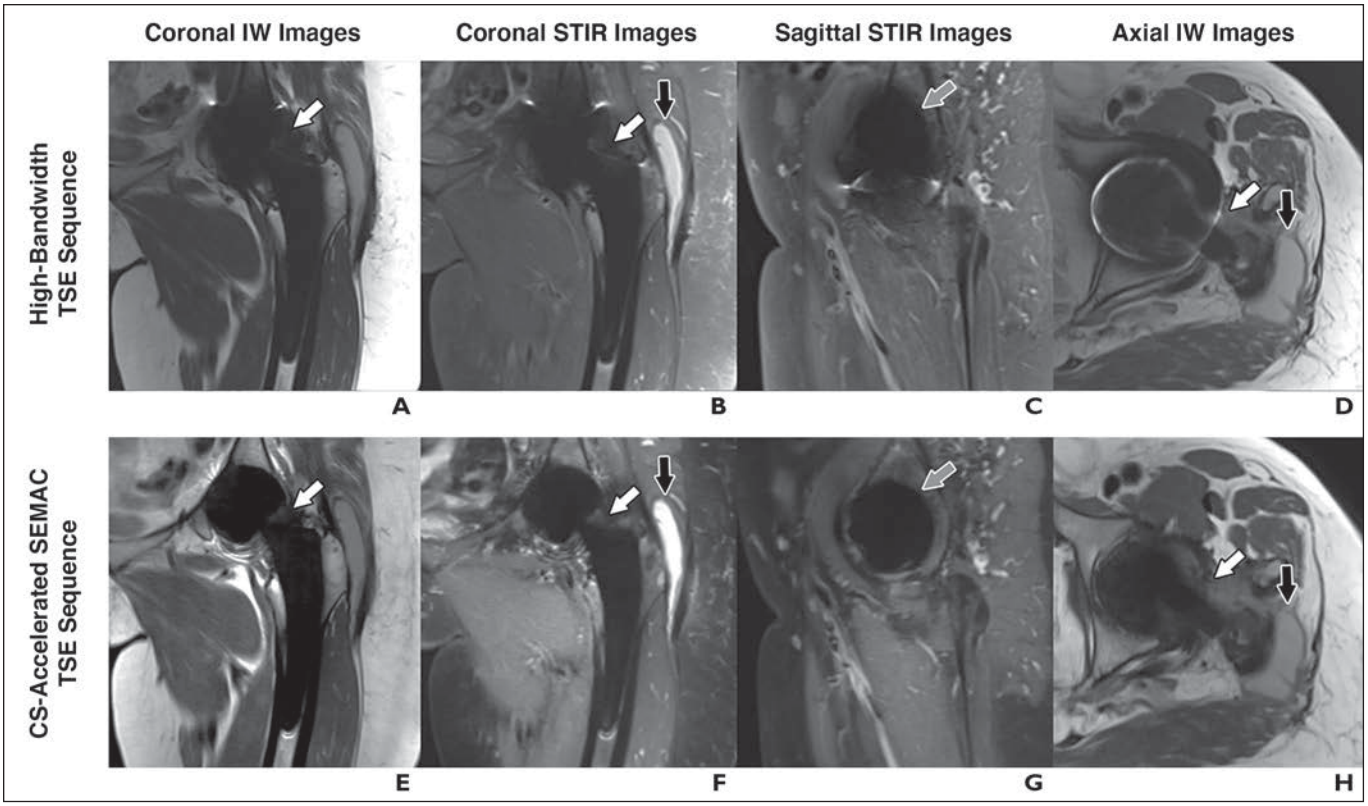

Fig. 8—64-year-old woman with pain and dysfunction of left hip who underwent metal artifact reduction MRI performed using 1.5-T system.
A–H, Eightfold compressed sensing (CS)-accelerated SEMAC (slice encoding for metal artifact correction) turbo spin-echo (TSE) MR images (**E**–**H**) show particulate synovitis (*white arrows*, **A**, **B**, **D**–**F**, and **H**) around neck of femoral component with fluid decompression into greater trochanteric bursa (*black arrows*, **B**, **D**, **F**, and **H**), and intact implant-bone interface (*arrows*, **C** and **G**) to better advantage than do high-transmit, high-receiver-bandwidth TSE MR images (**A**–**D**). Total acquisition time was 18 minutes for each of two protocols. IW = intermediate-weighted.

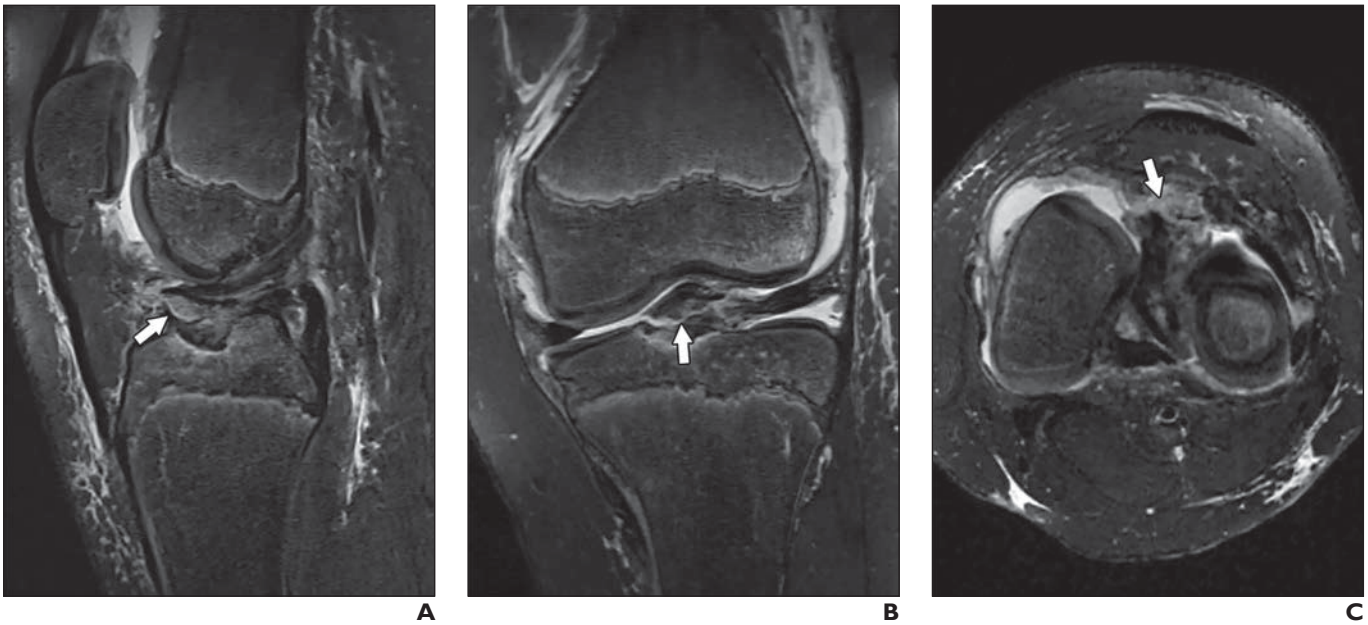

Fig. 9—11-year-old boy with acute knee trauma who underwent 3D compressed sensing–accelerated SPACE turbo spin-echo 3-T MRI examination of knee with acquisition time of 5 minutes.
A–C, Reformatted fat-suppressed, fluid-sensitive (spatial resolution, 0.5 × 0.5 × 0.5 mm) sagittal (**A**), coronal (**B**), and axial (**C**) MR images show osseous avulsion fracture (*arrows*) of tibial attachment of anterior cruciate ligament. Pulse sequence acquisition times without acceleration and with twofold acceleration are more than 20 minutes and more than 10 minutes, respectively.

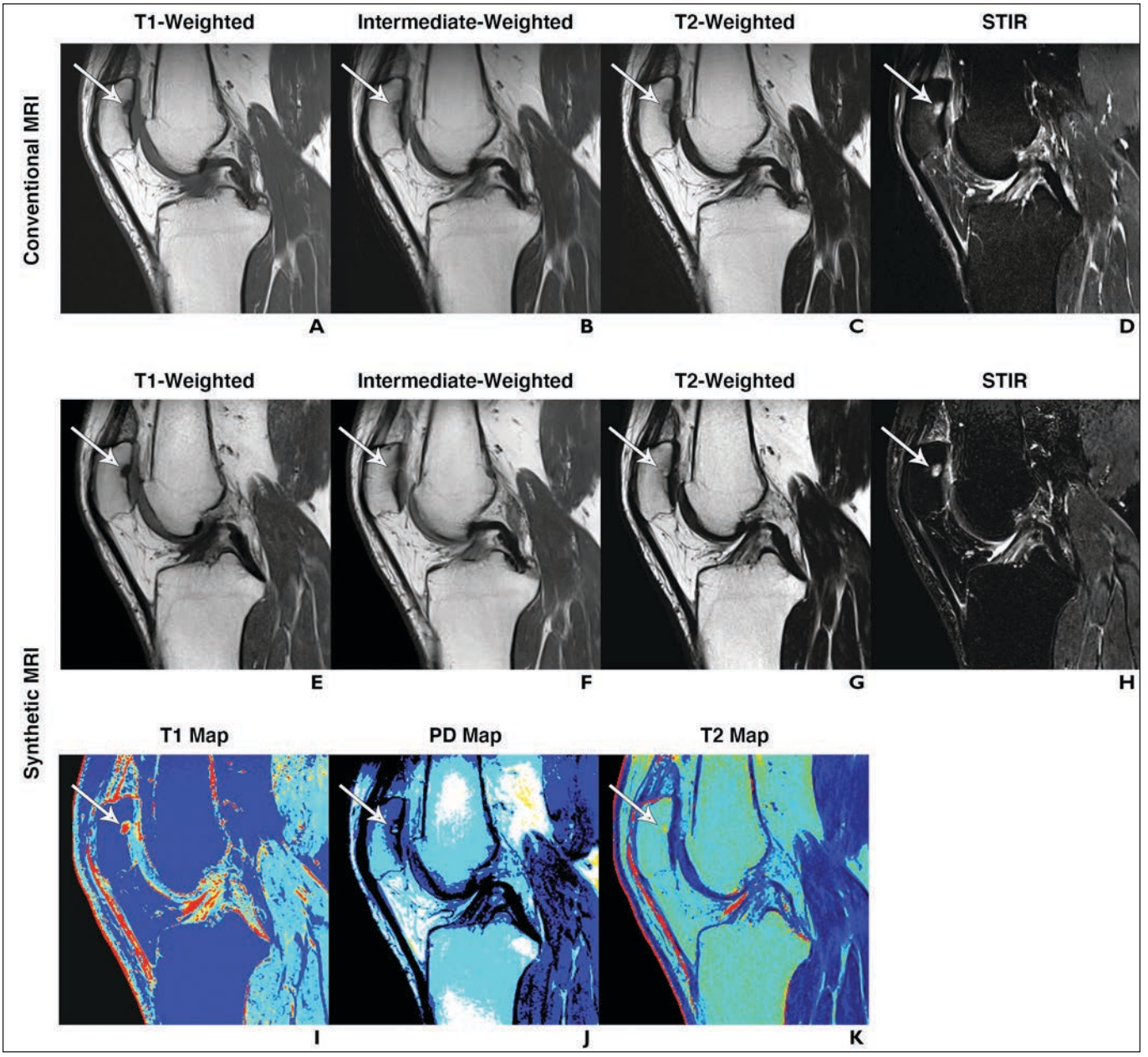

Fig. 10—28-year-old woman with right knee pain who underwent synthetic MRI.
A–**K,** Sagittal conventional MR images (**A**–**D**) and synthetic MR images (**E**–**H**) and T1 (**I**), proton density (**J**), and T2 (**K**) maps of knee show focal area of subchondral bone marrow edema (*arrow*) in central patella. PD = proton density.